# Optoacoustic System for 3D Functional and Molecular Imaging in Nude Mice

Matthew P. Fronheiser[a], Alan Stein [a], Don Herzog [a], Scott Thompson [a],
Anton Liopo [b], Mohammad Eghtedari [b], Massoud Motamedi [b],
Sergey Ermilov [c], Andre Conjusteau [c], Reda Gharieb [c], Ron Lacewell [c], Tom Miller [c], Ketan Mehta [c],
Alexander A. Oraevsky [*c],
[a]Seno Medical Instruments, San Antonio, TX USA;
[b]University of Texas Medical Branch, Galveston, TX USA;
[c]Fairway Medical Technologies, Houston, TX, USA;

## ABSTRACT

A three-dimensional laser optoacoustic imaging system was developed, which combines the advantages of optical spectroscopy and high resolution ultrasonic detection, to produce high contrast maps of optical absorbance in tissues. This system was tested in a nude mouse model of breast cancer and produced tissue images of tumors and vasculature. The imaging can utilize either optical properties of hemoglobin and oxyhemoglobin, which are the main endogenous tissue chromophores in the red and near-infrared spectral ranges, or exogenous contrast agent based on gold nanorods. Visualization of tissue molecules targeted by the contrast agent provides molecular information. Visulization of blood at multiple colors of light provides functional information on blood concentration and oxygen saturation. Optoacoustic imaging, using two or more laser illumination wavelengths, permits an assessment of the angiogenesis-related microvasculature, and thereby, an evaluation of the tumor stage and its metastatic potential.

The optoacoustic imaging system was also used to generate molecular images of the malignancy-related receptors induced by the xenografts of BT474 mammary adenocarcinoma cells in nude mice. The development of the latter images was facilitated by the use of an optoacoustic contrast agent that utilizes gold nanorods conjugated to monoclonal antibody raised against HER2/neu antigens. These nanorods possess a very strong optical absorption peak that can be tuned in the near-infrared by changing their aspect ratio. The effective conversion of the optical energy into heat by the gold nanorods, followed by the thermal expansion of the surrounding water, makes these nanoparticles an effective optoacoustic contrast agent. Optical scattering methods and x-ray tomography may also benefit from the application of this contrast agent. Administration of the gold nanorod bioconjugates to mice resulted in an enhanced contrast of breast tumors relative the background of normal tissues in the nude mouse model. The combination of this novel contrast agent and optoacoustic imaging has the potential to become a useful imaging modality, for preclinical research in murine models of cancer and other human diseases.

**Keywords:** Optoacoustic Imaging, functional imaging, molecular imaging, small animal imaging.

## 1. INTRODUCTION

Optoacoustic tomography (OAT) allows high resolution visualization of tissues with optical contrast based on endogenous chromophores in the near infrared spectrum [1]. It is one of a number of new and emerging functional imaging techniques. While anatomical imaging methods yield information related to the physical structure of a tissue, functional methods produce images based on the metabolic performance of a tissue, and may provide greater insight to researchers and clinicians interested in studying physiology and disease progression.

In optoacoustic imaging, absorption of laser illumination leads to selective energy deposition in absorbing tissues and generation of acoustic sources in regions with enhanced absorption. Short laser pulses (relative to the duration of pressure dissipation) are employed to stimulate the tissue. The induced localized temperature rise is accompanied by an effective pressure generation. The laser-induced pressure profile resembles the absorbed energy distribution in the irradiated tissue. A stronger absorption, as may be found in tumors, leads to a higher pressure amplitude and brighter image when compared with background signal from normal tissue.

*aoraevsky@fairwaymed.com; phone 1 713 722 7867; fax 1 713 772-2010; www.fairwaymed.com

Photons Plus Ultrasound: Imaging and Sensing 2008: The Ninth Conference on Biomedical Thermoacoustics, Optoacoustics, and Acousto-optics, edited by Alexander A. Oraevsky, Lihong V. Wang,
Proc. of SPIE Vol. 6856, 68560R, (2008) · 1605-7422/08/$18 · doi: 10.1117/12.770461

Detection and analysis of the acoustic waves allows reconstruction of three-dimensional optoacoustic distributions in the tissue either through back-projection of processed signals from wide-directivity transducers or direct detection of signals from voxels using focused transducers. Dual wavelength OA imaging uses 2 wavelengths in the near infrared (NIR) region. Differences in the spectral absorption of oxyhemoglobin and deoxyhemoglobin may be exploited to produce image contrast based on both total hemoglobin concentration as well as tissue oxygenation. OA techniques also possess the potential for use of exogenously administered highly absorbing contrast agents designed to target specific binding sites.

Seno Medical Instruments is developing a commercial optoacoustic small animal imaging system for researchers. This device will allow researchers to image phantoms and tissues with a high resolution functional technique. OA imaging is complementary to the other imaging techniques currently available to researchers, which include computed tomography (CT) x-ray, magnetic resonance imaging (MRI), single photon emission computed tomography (SPECT), positron emission tomography (PET), ultrasound (US), and optical techniques like fluorescence and bioluminescence. However OA offers the unique combination of a novel contrast mechanism, high resolution imagery, noninvasive and contrast free acquisitions, in a nonionizing technique.

The OA contrast mechanism is of particular relevance to cancer research because it is sensitive to hemoglobin concentration and oxygen saturation. In the early development of a malignant tumor, factors secreted into the surrounding tissue stimulate the growth of new blood vessels through a process known as angiogenesis. This produces localized regions of increased hemoglobin. Because rapid metabolic activity accompanies tumor growth, the lesions outgrow the blood supply producing regions of decreased oxygenation compared with surrounding tissue. Additionally, tumors also have other mechanisms that allow them to thrive in hypoxic (oxygen poor) environments [2].

Exogenous chromophores like gold nanorods may be tailored to provide high optical response targeted in a variety of ways. Conjugation to monoclonal antibodies provides contrast accumulation which is specific to expressed proteins analogous to other molecular imaging methods, but with the possibility of a high-resolution ultrasound-based readout. This system may be used to show the presence of specific cellular receptors or to demonstrate blocking of receptors by pharmalogical compounds [2]. In the absence of antibody specificity, such contrast agents will accumulate in tissues based on flow kinetics and may be used to enhance vasculature in a fashion similar to the microbubbles available for ultrasound study. Other contrast agents such as Indo-Cyanine Green (ICG) may also be used and may be of interest to researchers studying phamacokinetics.

Many groups have investigated using OA techniques to acquire very high resolution images. Early studies showed promising results when using OA tomography with lateral resolutions of 50 μm for detection and staging oral cancer [4,5]. Wang and his associates have investigated dual-wavelength photoacoustic tomography for both brain and subcutaneous microvascular purposes using high frequency (10-50MHz) ultrasonic detectors. These investigators have shown the ability to image brain and subcutaneous microvasculature with lateral resolutions as low as 50 μm. This group has also shown the functional imaging capabilities by using multiple wavelengths of light [6-9]. Most recently, Jung et. al reported imaging subcutaneous microvasculature at depths of a few millimeters using laser microferometer techniques [10].

Despite providing high resolution, these techniques lack the ability to penetrate to deeper imaging depths. Imaging the full body of the mouse could provide researchers with a tool to monitor metastatic activity from implanted tumor metastases or spontaneous growth. It could also allow investigators to examine the blood supply and oxygenation of deep organs and vessels. Very little literature exists for full body mouse imaging despite the demand for such a system. One group has published promising preliminary results from a prototype small animal imaging system designed for molecular imaging [11].

The authors are working on development of a commercial dual-wavelength optoacoustic imaging system capable of volumetric acquisition on phantoms and small animals. This system is being designed for functional imaging based on the presence of endogenous hemoglobin. This new imaging technique has applications in basic science research, investigation of physiology, pharmacokinetics, development of antiangiogenic compounds, and many other research areas. Advances in multidisciplinary knowledge between optics and acoustics as well as technological advances in lasers and acoustics detectors have made development of such a device a reality [12].

## 2. SYSTEM DESCRIPTION

Optoacoustic images of phantoms and nude mice were acquired using the IMAGIO small animal research imaging system (Seno Medical Devices, San Antonio, TX). The system uses a pulse-doubled Nd-YAG +Ti:Sa laser (Quanta System SPA, Olona, Italy), which can operate at either 775 nm or 1064 nm, for light delivery with a pulse duration less than 10 ns and a pulse repetition rate of 10 Hz. The light is introduced in the forward mode using an articulated arm and periscope or in the backward mode using bifurcated fiber bundles that are positioned on either side of the ultrasound detector.

The pressure waves created by the tissue response to the light are detected by a curved piezocomposite annular array that is designed to have equal area elements, a geometric focus of 25 mm, and 80% bandwidth. The light delivery system and ultrasound detector can be moved throughout the water tank by software using an XYZ translation stage at step sizes ranging from 0.1-1 mm. A rotary motor is also incorporated to permit specimen rotation if desired.

The signals are amplified by a custom built two-stage amplifier, with each stage providing a maximum of 48 dB of gain. After the amplification stage, the data is digitized by a 12-bit analog-to-digital converter with a maximum sampling rate of 104 MHz. The acquired channel data is combined using delay and sum methods. A set of A-lines created by moving the focused detector throughout an X-Y plane are used to create the volume of image data. The 3D dataset is displayed using Volview (Kitware, Clifton Park, NY).

## 3. PHANTOM EXPERIMENTS

The system was first tested using a small target phantom to investigate visualization of closely spaced targets. The phantom consisted of six horse hairs with an average diameter of 120 μm (Fig. 1a). These hairs were embedded at a depth of 7 mm in a heated plastisol mixture that contained titanium oxide to increase scattering. The six hairs were spaced 3 mm, 2 mm, 1 mm, 2 mm, and 3 mm apart. The phantom was positioned in the water tank so that the view from the detector matched that shown in Fig. 1a with the front surface positioned 20 mm from the detector and the hairs about 27 mm from the detector. Imaging was performed using 775 nm wavelength using the backward mode fiber bundles configuration described earlier with a translation step size of 0.3 mm. The angle between the beams was designed to have them overlap at 20 mm.

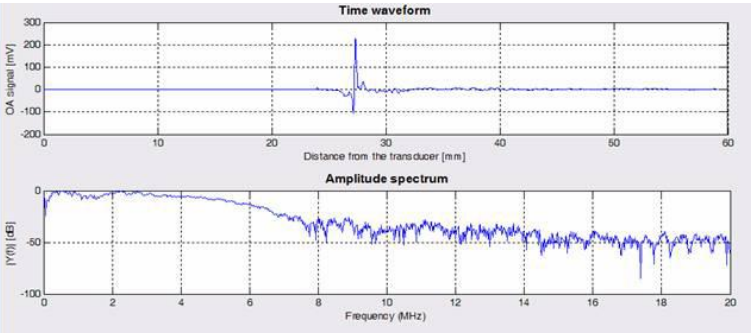


**Figure 1**: Plots showing typical A-line response from single horse hair and the corresponding frequency spectrum.

A typical beamformed A-line trace from a single horse hair in the phantom is shown in the top plot of Fig. 1, with the hair signal visible as a sharp spike. The frequency spectrum from this A-line is shown in the bottom plot of Fig. 1, with a broad spectrum resulting from the sharp spike. The final volume data from the scan is shown in Figs. 2b-d. The first slice, shown in Fig. 1b, shows an axial slice of the top hair in a long axis view. The coronal slice (Fig. 2c) was positioned to show four of the hairs in long axis. The top of the phantom was tilted slightly toward the detector, causing the hairs not to be perfectly aligned in the coronal plane. This is clear in the sagittal slice (Fig. 2d), where all six hairs are visible in cross section.

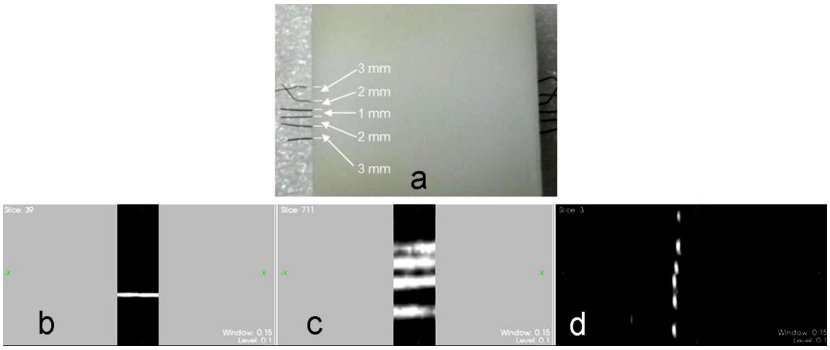


**Figure 2**. Picture of plastisol phantom with six horse hairs separated by varying distances (a). Axial slice shows top horse hair in long axis (b). Coronal slice shows 4 hairs in long axis (c). Sagittal slice shows all six hairs in short axis (d).

A second phantom consisting of a single 1 mm tube filled with cupric sulfate imbedded in a scattering plastisol background. This phantom was imaged to show the frequency dependence of the target size in OA imaging. Data was acquired using the 775 nm wavelength in the forward mode with a translation step size of 0.3 mm. A sample beamformed A-line and the associated frequency spectrum are shown below (Fig. 3). This pulse is broader than the hair phantom, which results in a frequency spectrum containing less high frequency content.

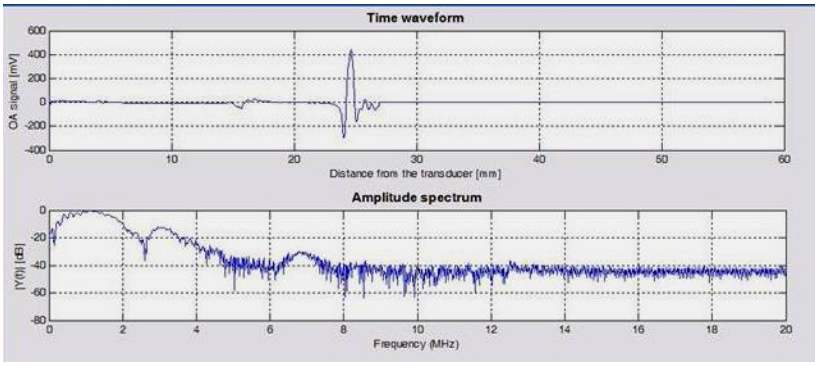


**Figure 3**: Sample A-line trace and corresponding frequency spectrum from 1mm tube with cupric sulfate.

The ability to visualize different shapes and multiple depths was tested using a clear plastisol phantom, 12 mm thick, with the letters IMAGIO written on the front surface (~23mm from detector) and SENO (~35 mm from detector) using a black Sharpie™ marker. Data were acquired in the backward mode using the 1064 nm wavelength while taking samples every 0.4 mm. Before processing, the data was filtered envelope detection on the beamformed A-lines. Figs. 4 a-b show the resulting image with the letters clearly visible on both surfaces. In addition, absorbing materials such as ink or paint could be used during phantom or mouse testing to provide reference points to help with orientation during image visualization.

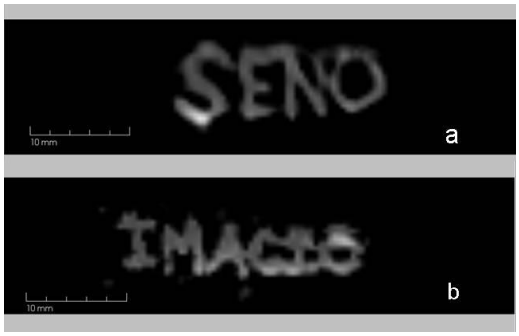


**Figure 4**: Images slices from plastisol phantom with letters written on front and back surface. The letters SENO and IMAGIO are clearly visible in both slices.

## 4. NUDE MOUSE EXPERIMENTS

Nude mice experiments were performed on 6-7 week old male mice with no cancer and on a 19 week old female mouse with a 9 week old tumor (tumor strand added). Before imaging, mouse preparation starts by anaesthetizing the mouse using isofluorene, which was delivered by our anaesthesia system. Once the mouse was unconscious, a subcutaneous dextrose injection was made and eye drops were applied. The mouse is mounted onto a plastic specimen holder that attaches to the translation stages of the imaging system. The holder is equipped with mounting holes to attach a nose cone anaesthesia delivery device to keep the mouse unconscious during experiments (Fig 5a). The mouse is mounted to the specimen holder by four holding pegs (Fig 5a). An example of the final mouse configuration is shown in Fig. 5b.

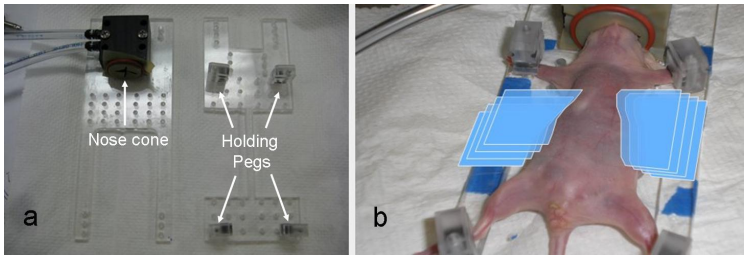


**Figure 5**. Picture showing two specimen holders with the nose cone and holding pegs (a). Final mouse configuration (b).

Both the forward and backward mode light delivery configurations were tested. A six week old male mouse was imaged in the forward mode using 1064 nm wavelength. The translation step size was set to 0.3 mm, the first stage of amplification was set to 20 dB of gain, and the second stage applied a varying gain with the illuminated surface (far from detector) receiving less amplification (20 dB) than the non-illuminated surface (40 dB). The collected channel data were processed to generate the A-line traces, which were filtered using a 2-MHz, 1$^{st}$ order Butterworth high pass filter and envelope detection (Fig. 6). The left hand side of the image shows the skin/water interface for the right hand side of the mouse. The abdominal aorta is visible in the middle of the mouse, as is the bifurcation to the femoral arteries.

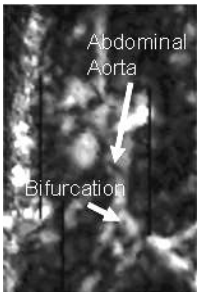


**Figure 6**. Forward mode acquired coronal slice showing abdominal aorta and a bifurcation.

The potential of dual wavelength imaging is illustrated in the images acquired during the scan of an 18 week old female mouse with BT474 human breast cancer xenograft. The tumor was located on the back right side of the animal. Data were acquired in the backward mode with a 0.3 mm step size over the tumor area using both the 775 nm and 1064 nm wavelengths. Images were coregistered and compared with similar brightness and contrast settings. Figs. 7a-c show the axial, coronal, and sagittal slices from the 1064 nm data while Fig. 7d-f shows the same slices for the 775 nm data. In Fig. 7d-f a bright intensity region is present that is not in the 1064 nm data slices, indicating that the region has a lower oxygenation level from the surrounding tissue.

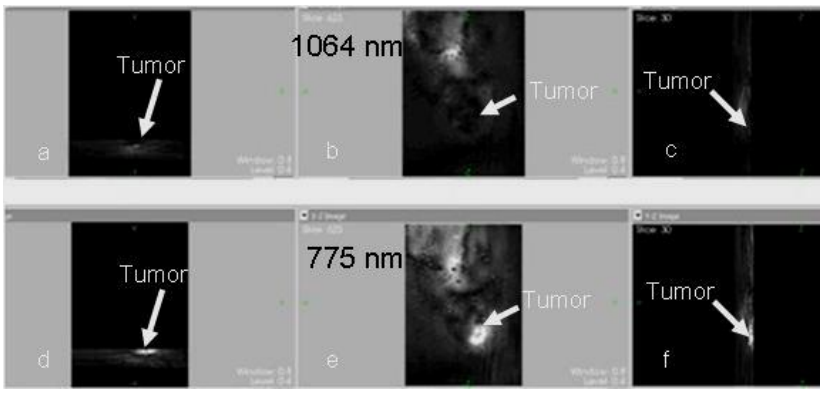


**Figure 7**. Dual wavelength capability displayed by the increased tumor signal at the 775 nm wavelength when compared to the 1064 nm wavelength.

Molecular imaging using OA techniques and gold nanorods contrast agents was investigated and is shown below. In this case, the gold nanorods are peaked for the near-infrared by modification of the aspect ratio. These structures are very effective in converting light to heat, which then causes the thermal expansion of the surrounding water. Nanorods were injected into a tail vein into a mouse with a BT474 mouse tumor and accumulated in the targeted tumor. Image data was acquired in the forward mode (posterior side of animal illuminated) using 0.3 mm steps to acquire the volume of data. The posterior outline of the mouse is clearly visible in the coronal image slice (Fig 8a). Also visible is an area of higher intensity, which represents the mouse tumor. The tumor visibility is enhanced by the uptake of the gold nanorods. A slice more anterior (Fig. 8b) shows the right and left kidneys with increased signals due to the collection of the nanoparticles.

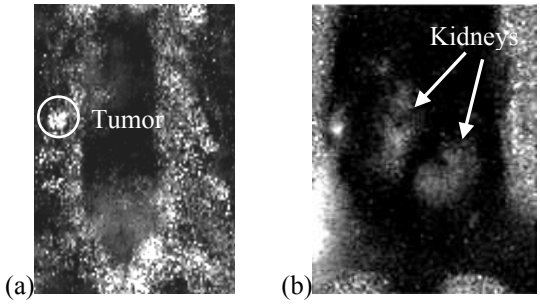


**Figure 8.** Increased signals from tumor after uptake from nanoparticles (a). Increased signals from kidneys in same mouse after nanorod uptake (b).

## 5. DISCUSSION

In designing the OA system, several engineering tradeoffs must be considered. The difficulties in working with wideband ultrasonic detectors are contrasted against the restricted bandwidth but better availability of piezo-ceramic elements. In choosing a ceramic material, the selection of center frequency involves assessment of competing effects. Acoustic propagation attenuates at approximately 2-4db/Mhz/cm, so there is a desire to select low-frequency components (e.g. < 5 MHz) to minimize attenuation of OA signals which originate several cm deep within the sample. However, the acoustic spectral response is directly related to the sample structure. Selection of a detector with low central frequency substantially restricts the system ability to resolve small structural features. In similar fashion, multiple detector configurations are possible. Simplistic fixed focus detectors have easily characterized profiles, minimal supporting hardware requirements, and longer scans times, when compared with sophisticated 1D and 2D arrays that can provide advanced signal detection and shorter scan times at the expense of multi channel support hardware and more complicated reconstruction techniques. Lastly, a variety of illumination techniques exist and must be considered with respect to laser fluence, illumination homogeneity, difficulty of construction, and illumination area.

The development of an optoacoustic imaging system designed for small animal research will provide a valuable tool for investigators in a variety of fields. The work presented here shows the internal structures of a nude mouse, the advantages of using a dual wavelength system when examining tumors, and the potential of molecular imaging when

combining OA techniques with gold nanorods. These results show the potential of OA imaging in a variety of fields. Work is ongoing to improve our current performance. System refinements are being investigated to optimize our system to improve the imaging depth and resolution during animal imaging. Other areas of focus include advancements in phantom design, transducer design, signal processing, and investigation into the correlation of the pathophysiology with the structures visualized in the images.

## ACKNOWLEDGEMENT

This work was supported in part by the National Cancer Institute, grant # R44CA110137.

## REFERENCES

[1] Oraevsky, A.A., Karabutov A.A. "Optoacoustic Tomography ", in Biomedical Photonics Handbook, ed. By T. Vo-Dinh, CRC Press, 2003, Vol. PM125, Chapter 34, pp. 34/1-34/34.

[2] Vaupel, P., Mayer, A., Hockel, M., "Tumor Hypoxia and Malignant Progression," Methods in Enzymology 381, 335-354 (2004)

[3] Eghtedari, M., Oraevsky, A., Copland, J.A., Kotov, N.A., Conjusteau, A., Motamedi, M., "High Sensitivity of *in vivo* Detection of Gold Nanorods Using a Laser Optoacoustic Imaging System," Nano Lett 7(7), 1914-1918 (2007)

[4] Oraevsky, A.A., Karabutov, A.A., Savateeva, E.B., Bell, B., Motamedi, M., Thomsen, S., Pasricha, P.J., "Opto-acoustic imaging of oral cancer: Feasibility studies in hamster model of squamous cell carcinoma," Proc. SPIE 3597, 385-396 (1999)

[5] Savateeva, E., Karabutov, A., Motamedi, M., Bell, B., Johnigan, R., Oraevsky, A., "Noninvasive detection and staging of oral cancer *in vivo* with confocal opto-acoustic tomography," Proc. SPIE 3916, 55-66 (2000)

[6] Wang, X., Xie, X., Ku, G., Wang, L.V., "Noninvasive imaging of hemoglobin concentration and oxygenation in the rat brain using high-resolutionphotoacoustic tomography," Journal of Biomedical Optics 11(2), 024015-1 – 024015-9 (2006)

[7] Zhang, H.F., Maslov, K., Stoica, G., Wang, L.V., "Functional photoacoustic microscopy for high-resolution and noninvasive *in vivo* imaging," Nature Biotechnology 24(7), 848-851 (2006)

[8] Oh, J.T., Li, M.L., Zhang, H.F., Maslov, K., Stoica, G., Wang, L.V., "Three-dimensional imaging of skin melanoma *in vivo* by dual-wavelength photoacoustic microscopy," Journal of Biomedical Optics 11(3), 034032-1 – 034032-4 (2006)

[9] Zhang, H.F., Maslov, K., Wang, L.V., "*In vivo* imaging of subcutaneous structures using functional photoacoustic microscopy," Nature Protocols 2, 797-804 (2007)

[10] Zhang, E., Laufer, J., Beard, P., "Backward-mode multiwavelength photoacoutic scanner using a planar Fabry-Perot polymer film ultrasound sensor for high-resolution three-dimensional imaging of biological tissues," Applied Optics 47(4), 561-577 (2008)

[11] Kruger, R.A., Kiser, W.L., Reinecke, D.R., Kruger, G.A., Miller, K.D., "Thermoacoustic Molecular Imaging of Small Animals," Molecular Imaging 2(2), 113-123 (2003)

[12] Andreev, V.G., Karabutov, A.A. , Oraevsky, A.A., "Detection of ultrawide-band ultrasound pulses in optoacoustic tomography," IEEE Trans. Ultrason Ferroelectr Freq Control, 50(10), 1383-1391 (2003).